
Learning Long Range Dependencies on Graphs via Random Walks

Dexiong Chen Till Hendrik Schulz Karsten Borgwardt
Max Planck Institute of Biochemistry
82152 Martinsried, Germany
{dchen, tschulz, borgwardt}@biochem.mpg.de

Abstract

Message-passing graph neural networks (GNNs), while excelling at capturing local relationships, often struggle with long-range dependencies on graphs. Conversely, graph transformers (GTs) enable information exchange between all nodes but oversimplify the graph structure by treating them as a set of fixed-length vectors. This work proposes a novel architecture, NeuralWalker, that overcomes the limitations of both methods by combining random walks with message passing. NeuralWalker achieves this by treating random walks as sequences, allowing for the application of recent advances in sequence models in order to capture long-range dependencies within these walks. Based on this concept, we propose a framework that offers (1) more expressive graph representations through random walk sequences, (2) the ability to utilize any sequence model for capturing long-range dependencies, and (3) the flexibility by integrating various GNN and GT architectures. Our experimental evaluations demonstrate that NeuralWalker achieves significant performance improvements on 19 graph and node benchmark datasets, notably outperforming existing methods by up to 13% on the PascalVoc-SP and COCO-SP datasets.

Code: <https://github.com/BorgwardtLab/NeuralWalker>.

1 Introduction

Graphs are a powerful data structure for representing complex interactions and relationships within data. However, traditional machine learning models, primarily designed for vector-based data, are not inherently suited for processing graph-structured data. Recently, graph learning methods, such as message-passing graph neural networks (GNNs) [19] and graph transformers (GTs) [51], have emerged as powerful tools for exploiting these structures. These advancements in graph learning have broad implications, impacting fields such as social network analysis [16], physics [37, 40] and bioinformatics [24, 42].

Most graph learning methods face inherent challenges in modeling long-range dependencies on graphs. Popular message-passing GNNs [19, 50] often fail to capture distant relationships due to the local nature of message passing, leading to issues such as over-smoothing [36] and over-squashing [2]. In contrast, GTs [51, 32, 9, 39, 41] address these limitations by directly modeling long-range interactions through global attention mechanisms, allowing information exchange between all nodes. However, GTs typically preprocess the complex graph structure into (node-wise) fixed-length vectors through positional or structural encodings [39], thereby treating the graph essentially as a set of nodes enriched with these vectors. This fixed-length vector representation inevitably leads to a loss of structural information, limiting expressivity even when GTs are combined with local message-passing techniques [53]. In this work, we address these limitations by introducing a novel architecture that can capture long-range dependencies while retaining rich structural information, by leveraging the power of random walks combined with message passing.

Instead of representing the graph structure as fixed-length vectors, random walks offer a flexible approach to exploring graphs. By traversing diverse paths across the graph, random walks can capture long-range dependencies that are likely to be missed by message passing. Furthermore, they can capture subgraphs and relationships, such as cycles, that are generally not identifiable by local message passing, as illustrated in Figure 1. More importantly, the complexity of random walks is determined by their length and sample size rather than the size of the graph, making them scalable for representing large graphs. Although some previous models are based on random walks, they have notable limitations. Some focus solely on short walks [8, 35], while others use them for structural encoding, neglecting the rich information they hold [14, 32]. A recent method, CRaWL [45], shows promise by representing a graph as a set of random walks. However, its reliance on a convolutional layer to process random walks, particularly with small kernel sizes, limits its ability to capture long-range dependencies within each walk fully.

Motivated by the limitations of positional or structural encodings and shortcomings of existing random-walk-based models, we introduce a novel architecture that leverages the strengths of both paradigms (random walks and message passing). Rather than encoding random walks into fixed-length vectors as done in GTs [39, 9], we preserve their sequential nature, thus retaining richer structural information. This architecture, named **NeuralWalker**, samples random walks with a predefined sampling rate and length, then uses advanced sequence models to process them. Additionally, local and global message passing can be employed to capture complementary information. To our knowledge, we are the first to use long sequence models, such as state space models, on random walk sequences.

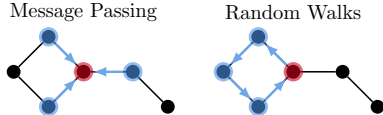


Figure 1: Message passing captures degree centrality information while random walks capture subgraphs like cycles.

Our contributions are summarized as follows. i) We propose a novel framework that leverages both random walks and message passing, enabling a more expressive graph representation by treating graphs as sets of sequences (random walks). This allows the model to exploit advances in sequence modeling (transformers, state space models, etc.) to capture long-range dependencies within the walks. ii) Our message-passing block can seamlessly integrate various GNN and GT architectures, allowing for customization based on specific tasks. iii) We conduct extensive ablation studies to offer practical insights for choosing the optimal sequence layers and message-passing blocks. Notably, the trade-off between model complexity and expressivity can be controlled by adjusting sampling rate and walk length hyperparameters. iv) Our model demonstrates significant performance improvements over existing methods on a comprehensive set of 19 graph and node benchmark datasets.

2 Related Work

Local and global message passing. Message-passing neural networks (MPNNs) are a cornerstone of graph learning. They propagate information between nodes, categorized as either local or global methods based on the propagation range. Local MPNNs, also known as GNNs (e.g. GCN [26], GIN [50]), excel at capturing local relationships but struggle with distant interactions due to limitations like over-smoothing [36] and over-squashing [2]. Global message passing offers a solution by modeling long-range dependencies through information exchange across all nodes. GTs [51, 27, 32, 9, 39, 41], using global attention mechanisms, are a prominent example. However, GTs achieve this by compressing the graph structure into fixed-length vectors, leading to a loss of rich structural information. Alternative techniques include the virtual node approach [19, 3], which enables information exchange between distant nodes by introducing an intermediary virtual node.

Random walks for graph learning. Random walks have a long history in graph learning, particularly within traditional graph kernels. Due to the computational intractability of subgraph or path kernels [18], walk kernels [18, 25, 5] were introduced to compare common walks or paths in two graphs efficiently. Non-backtracking walks have also been explored [31] for molecular graphs. In deep graph learning, several approaches utilize walks or paths to enhance GNN expressivity. GCKN [8] pioneered short walk and path feature aggregation within graph convolution, further explored in [33]. RWGNN [35] leverages differentiable walk kernels for subgraph comparison and parametrized anchor graphs. The closest work to ours is CRaWL [44]. However, it lacks message passing and relies on a convolutional layer, particularly with small kernel sizes, limiting its ability to

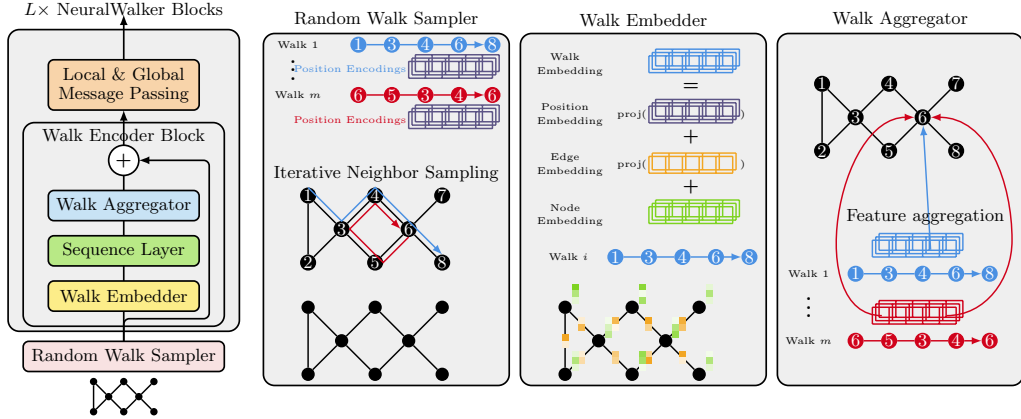


Figure 2: Overview of the NeuralWalker architecture. The random walk sampler samples m random walks independently without replacement; the walk embedder computes walk embeddings given the node/edge embeddings at the current layer; the walk aggregator aggregates walk features into the node features via pooling of the node features encountered in all the walks passing through the node.

capture long-range dependencies within each walk. Additionally, random walks have been used as structural encoding in GTs such as RWPE [14] and relative positional encoding in self-attention [32].

Sequence modeling. Sequence models, particularly transformers [46] and state space models (SSMs) [21, 20], have become instrumental in natural language processing (NLP) and audio processing due to their ability to capture long-range dependencies within sequential data. However, directly leveraging these models on graphs remains challenging due to the inherent structural differences. Existing approaches like GTs treat graphs as sets of nodes, hindering the application of transformer architectures to sequences within the graph. Similarly, recent work utilizing SSMs for graph modeling [48, 4] relies on node ordering based on degrees, a suboptimal strategy that may introduce biases or artifacts when creating these artificial sequences that do not reflect the underlying graph topology.

Our work addresses this limitation by explicitly treating random walks on graphs as sequences. This allows us to leverage the power of state-of-the-art (SOTA) sequence models to capture rich structural information within these walks, ultimately leading to a more expressive graph representation.

3 Neural Walker

In this section, we propose the neural architecture operating on sequences based on random walks to obtain node and graph representations. The main components of the proposed NeuralWalker consist of a random walk sampler (Section 3.2) and a stack of neural walker blocks with a walk encoder block and a message passing block. Each walk encoder block has a walk embedder, a sequence layer, and a walk aggregator (Section 3.3, 3.4, 3.5). A visualization of NeuralWalker’s architecture can be found in Figure 2.

3.1 Notation and Random Walks on Graphs

We first introduce the necessary notation. A graph is a tuple $G = (V, E, x, z)$, where V is the set of nodes, E is the set of edges, and $x : V \rightarrow \mathbb{R}^d$ and $z : E \rightarrow \mathbb{R}^{d'}$ denote the functions assigning attributes to node and edges, respectively. We denote by \mathcal{G} and \mathcal{G}_n the space of all graphs and the space of graphs up to size n , respectively. The neighborhood of a node v is denoted by $\mathcal{N}(v)$ and its degree by $d(v)$. A walk W of length ℓ on a graph G is a sequence of nodes linked with edges, i.e. $W = (w_0, \dots, w_\ell) \in V^{\ell+1}$ such that $w_{i-1}w_i \in E$ for all $i \in [\ell]$. We denote by $\mathcal{W}(G)$ and $\mathcal{W}_\ell(G)$ the set of all walks and all walks of length ℓ on G , respectively. W is called non-backtracking if $w_{i-1} \neq w_{i+1}$ for any i and we denote the set of all such walks of length ℓ by $\mathcal{W}_\ell^{\text{nb}}(G)$. A random walk is a Markov chain that starts with some distribution on nodes $P_0(v)$ and transitions correspond to moving to a neighbor chosen uniformly at random. For non-backtracking random walks, neighbors are chosen uniformly from $\mathcal{N}(w_i) \setminus \{w_{i-1}\}$. We denote by $P(\mathcal{W}(G), P_0)$ the distribution of random

walks with initial distribution P_0 , and by $P(\mathcal{W}(G))$ the case where $P_0 = \mathbb{U}(V)$ is the uniform distribution on V .

3.2 Random Walk Sampler

A random walk sampler independently samples a subset of random walks on each graph through a probability distribution on all possible random walks. For any distribution on random walks $P(\mathcal{W}(G), P_0)$, we denote by $P_m(\mathcal{W}(G)) := \{W_1, \dots, W_m\}$ a realization of m i.i.d. samples $W_j \sim P(\mathcal{W}(G), P_0)$. Our model is always operating on such realizations. In this work, we consider two simple yet effective random walk samplers, by noting that more efficient sampling strategies with faster graph coverage are left for future work. Particularly, we consider the uniform distribution of length- ℓ random walks $P(\mathcal{W}(G), P_0) := P(\mathcal{W}_\ell(G), \mathbb{U}(V))$ and, furthermore, the non-backtracking variant $P(\mathcal{W}(G), P_0) := P(\mathcal{W}_\ell^{\text{nb}}(G), \mathbb{U}(V))$. Motivated by the halting issue in random walks of arbitrary length, where a weight with each random walk decays with its length, we use non-backtracking random walks of *fixed* length in all our experiments. Note that one could also consider a stationary initial distribution $P_0(v) = d^{(v)}/2|E|$ for better theoretical properties [30].

In practice, we restrict $m \leq n$ where $n = |V|$ for computation efficiency. To maximize the coverage, we sample each walk from a different start node to ensure that our realization is without replacement. We define the sampling rate of random walks as the ratio of random walks to nodes ($\gamma := m/n$). While paths (defined as walks without repeated nodes) could also be considered, they are often too short on sparse graphs, resulting in limited graph coverage and thus failing to capture long-range dependencies. Notice that random walks only need to be sampled once for each forward pass, and that an efficient CPU implementation can be achieved through iterative neighbor sampling. During inference, a higher sampling rate than that used during training can be used to enhance performance.

Positional encodings for random walks. Similar to [45], we use additional encoding features that store connectivity information captured during random walks. In particular, we consider an identity encoding which encodes whether two nodes in a walk are identical within a window and an adjacency encoding which includes information about subgraphs induced by nodes along the walk. Specifically, for any length- ℓ walk $W = (w_0, \dots, w_\ell) \in \mathcal{W}_\ell(G)$ and a window size $s \in \mathbb{N}_+$, the identity encoding id_W^s of W for the window size s is a binary vector in $\{0, 1\}^{(\ell+1) \times s}$ such that $\text{id}_W^s[i, j] = 1$ if $w_i = w_{i-j-1}$ and $i - j \geq 1$ otherwise 0 for any $0 \leq i \leq \ell$ and $0 \leq j \leq s - 1$. Similarly, the adjacency encoding $\text{adj}_W^s \in \{0, 1\}^{(\ell+1) \times (s-1)}$ satisfies that $\text{adj}_W^s[i, j] = 1$ if $w_i w_{i-j-1} \in E$ and $i - j \geq 1$ otherwise 0 for any $0 \leq i \leq \ell$ and $0 \leq j \leq s - 1$. We concatenate all encodings into a single matrix $h_{\text{pe}} \in \mathbb{R}^{(\ell+1) \times d_{\text{pe}}}$ together with the sampled random walks as the output of the random walk sampler. A visual example of these encodings is given in Appendix B.1.

Although the positional encoding from Transformers [46] could be used to represent relative node locations within the walk, our experiments did not show any performance gains with its inclusion.

3.3 Walk Embedder

The walk embedder in each walk encoder block generates walk embeddings given the sampled walks, and the node and edge embeddings at the current layer. It is defined as a function $f_{\text{emb}} : \mathcal{W}_\ell(G) \rightarrow \mathbb{R}^{(\ell+1) \times d}$. Specifically, for any sampled walk $W \in P_m(\mathcal{W}_\ell(G))$, the walk embedding $h_W := f_{\text{emb}}(W) \in \mathbb{R}^{(\ell+1) \times d}$ is defined as

$$h_W[i] := h_V(w_i) + \text{proj}_{\text{edge}}(h_E(w_i w_{i+1})) + \text{proj}_{\text{pe}}(h_{\text{pe}}[i]), \quad (1)$$

where $h_V : V \rightarrow \mathbb{R}^d$ and $h_E : E \rightarrow \mathbb{R}^{d_{\text{edge}}}$ are node and edge embeddings at the current block and $\text{proj}_{\text{edge}} : \mathbb{R}^{d_{\text{edge}}} \rightarrow \mathbb{R}^d$ and $\text{proj}_{\text{pe}} : \mathbb{R}^{d_{\text{pe}}} \rightarrow \mathbb{R}^d$ are some trainable projection functions. The resulting walk embeddings can then be processed with any sequence model as discussed below.

3.4 Sequence Layer on Walk Embeddings

Any sequence model can be used to process the walk embeddings obtained above. A sequence layer transforms a sequence of feature vectors into a new sequence, *i.e.*, a function $f_{\text{seq}} : \mathbb{R}^{(\ell+1) \times d} \rightarrow \mathbb{R}^{(\ell+1) \times d}$. Below, we list several possible choices for such a function.

1D CNNs are simple and fast models that process sequences, also used in [45]. They are GPU-friendly and require relatively limited memory. However, the receptive field of a 1D CNN is limited by its kernel size, which might fail to capture distant dependencies on long walks.

Transformer models are widely used in modeling long sequences and large graphs due to their universality and strong empirical performance. In recent years, a vast family of efficient transformers has been proposed to reduce the quadratic dependence on sequence length in NLP, also showing promising results in graph learning. However, we found in our experiments that they are suboptimal encoders for walk embeddings, even though equipped with positional encodings such as RoPE [43].

SSMs are more recent models for modeling long sequences. In our experiments, we tested two latest instances of SSMs, namely S4 [21] and Mamba [20]. In addition to the original version, we consider the bidirectional version of Mamba [52]. We found that bidirectional Mamba consistently outperforms other options (Section 5.2). Appendix A.3 provides more background of SSMs.

3.5 Walk Aggregator

A walk aggregator aggregates walk features into node features such that the resulting node features encode context information from all walks passing through that node. It is defined as a function $f_{\text{agg}} : (P_m(\mathcal{W}_\ell(G)) \rightarrow \mathbb{R}^{(\ell+1) \times d}) \rightarrow (V \rightarrow \mathbb{R}^d)$ and the resulting node feature mapping is given by $h_V^{\text{agg}} := f_{\text{agg}}(f_{\text{seq}}(f_{\text{emb}}|_{P_m(\mathcal{W}_\ell(G))}))$ where $f|_A$ denotes the function restriction. In this work, we consider the average of all the node features encountered in the walks passing through that node. Specifically, the resulting node feature mapping h_V^{agg} through average pooling is then given by

$$h_V^{\text{agg}}(v) := \frac{1}{N_v(P_m(\mathcal{W}_\ell(G)))} \sum_{W \in P_m(\mathcal{W}_\ell(G))} \sum_{w_i \in W \text{ st. } w_i=v} f_{\text{seq}}(h_W)[i], \quad (2)$$

where $N_v(P_m(\mathcal{W}_\ell(G)))$ represents the number of occurrences of v in the union of walks in $P_m(\mathcal{W}_\ell(G))$. One could also average the edge features in the walks passing through a certain edge to update the edge features: $h_E^{\text{agg}}(e) := \sum_{W \in P_m(\mathcal{W}_\ell(G))} \sum_{w_i w_{i+1} \in W \text{ st. } w_i w_{i+1}=e} f_{\text{seq}}(h_W)[i]$ up to a normalization factor. In practice, we also use skip connections to keep track of the node features from previous layers.

3.6 Local and Global Message Passing

While random walks with the above encodings are able to detect small subgraphs such as cycles, they lack the ability to effectively capture centrality information, a task at which message passing excels [45]. We, therefore, include a message passing layer into our encoder block to further improve the expressivity. Such a layer consists of either local or global message passing or both of them. Specifically, the local message passing step can be expressed as:

$$h_V^{\text{mp}}(v) := h_V^{\text{agg}}(v) + \text{MPNN}(G, h_V^{\text{agg}}(v)), \quad (3)$$

where MPNN denotes any GNN model, typically with one layer. We analyze the impact of using different local and global message passing layers in Section 5.2.

After a local message passing step, one could also apply a global message passing to incorporate global information into nodes by allowing all pairs of nodes to exchange information, as in GTs [9]. Even though long random walks could be sufficient to capture global information, we empirically found that global message passing is still useful in certain tasks. Similar to [19, 45], a virtual node layer could be a simple solution to achieve this. Such a layer is explicitly defined as the following:

$$h_V^t(\star) = \text{MLP} \left(h_V^{t-1}(\star) + \sum_{v \in V} h_V^{\text{mp}}(v) \right), \quad h_V^{\text{vn}}(v) := h_V^{\text{mp}}(v) + h_V^t(\star), \quad (4)$$

where MLP is a trainable MLP, $h_V^t(\star)$ represents the virtual node embedding at block t and $h_V^0(\star) = 0$. Alternatively, one could use any transformer layer to achieve this. The vanilla transformer layer is given by:

$$h_V^{\text{attn}}(v) = h_V^{\text{mp}}(v) + \text{Attn}(h_V^{\text{mp}}(v)), \quad h_V^{\text{trans}}(v) = h_V^{\text{attn}}(v) + \text{MLP}(h_V^{\text{attn}}(v)), \quad (5)$$

where Attn is a trainable scaled dot-product attention layer [46]. This layer is widely used in recent GT models [51, 9, 39]. Appendix A.2 provides more background of graph transformers.

4 Theoretical Results

In this section, we investigate the theoretical properties of NeuralWalker. The proofs of the following results as well as more details can be found in Appendix C.

We first define walk feature vectors following [45]:

Definition 4.1 (Walk feature vector). *For any graph $G = (V, E, x, z)$ and $W \in \mathcal{W}_\ell(G)$, the walk feature vector X_W of W is defined by concatenating the node and edge feature vectors, along with the positional encodings of W of window size $s = \ell$. Formally,*

$$X_W = (x(w_i), z(w_i w_{i+1}), h_{pe}[i])_{i=0, \dots, \ell} \in \mathbb{R}^{(\ell+1) \times d_{\text{walk}}},$$

where h_{pe} represents the positional encoding in Section 3.2, $z(w_\ell w_{\ell+1}) = 0$, and $d_{\text{walk}} := d + d' + d_{pe}$. For simplicity, we still denote the distribution of walk feature vectors on G by $P(\mathcal{W}(G))$.

Now assume that we apply an average pooling followed by a linear layer to the output of the walk aggregator in Eq. (1). By adjusting the normalization factor to a constant $m^\ell/|V|$, we can express the function $g_{f,m,\ell}$ on \mathcal{G} as an average over functions of walk feature vectors:

$$g_{f,m,\ell}(G) = \frac{1}{m} \sum_{W \in P_m(\mathcal{W}_\ell(G))} f(X_W) \quad (6)$$

where $f : \mathbb{R}^{d_{\text{walk}}} \rightarrow \mathbb{R}$ is some function on walk feature vectors.

If we sample a sufficiently large number of random walks, the average function $g_{f,m,\ell}(G)$ converges almost surely to $g_{f,\ell} := \mathbb{E}_{X_W \sim P(\mathcal{W}_\ell(G))}[f(X_W)]$, due to the law of large numbers. This result can be further quantified using the central limit theorem, which provides a rate of convergence (see Theorem C.7 in Appendix). Furthermore, we have the following useful properties of the limit:

Theorem 4.2 (Lipschitz continuity). *For some functional space \mathcal{F} of functions on walk feature vectors, we define the following distance $d_{\mathcal{F}} : \mathcal{G} \times \mathcal{G} \rightarrow \mathbb{R}_+$:*

$$d_{\mathcal{F},\ell}(G, G') := \sup_{f \in \mathcal{F}} \left| \mathbb{E}_{X_W \sim P(\mathcal{W}_\ell(G))}[f(X_W)] - \mathbb{E}_{X_{W'} \sim P(\mathcal{W}_\ell(G'))}[f(X_{W'})] \right|. \quad (7)$$

Then $(\mathcal{G}_n, d_{\mathcal{F},\ell})$ is a metric space if $\ell \geq 4n^3$.

If \mathcal{F} contains f , then for any $G, G' \in \mathcal{G}_n$, we have

$$|g_{f,\ell}(G) - g_{f,\ell}(G')| \leq d_{\mathcal{F},\ell}(G, G'). \quad (8)$$

Theorem 4.3 (Injectivity). *Assume that \mathcal{F} is a universal space. If G and G' are non-isomorphic graphs, then there exists an $f \in \mathcal{F}$ such that $g_{f,\ell}(G) \neq g_{f,\ell}(G')$ if $\ell \geq 4 \max\{|V|, |V'|\}^3$.*

The Lipschitz continuity implies that NeuralWalker is stable to small perturbations in the graph structure, ensuring robustness in its predictions. The injectivity property ensures that our model with a sufficiently large number of sufficiently long ($\geq 4n^3$) random walks can distinguish between non-isomorphic graphs, highlighting its expressive power.

As the above result requires long random walks, we now provide a weaker expressivity result without this assumption. Specifically, we show that due to its powerful positional encoding, NeuralWalker can directly be linked to the family of MPNNs enriched with subgraph counts. The following theorem is derived from NeuralWalker’s capability to identify induced subgraphs. Analogously to [6], we show that performing message passing on node embeddings enhanced by this subgraph information increases the expressive power over ordinary message passing neural networks.

Theorem 4.4. *For any $\ell \geq 2$, NeuralWalker equipped with the complete walk set \mathcal{W}_ℓ is strictly more expressive than 1-WL, and thus ordinary MPNNs.*

Notice that the above theorem requires a complete walk set of size ℓ in order to ensure deterministic node representations. It is easy to see that already for $\ell = 2$, NeuralWalker can identify and count triangles which ordinary MPNNs are not capable of.

5 Experiments

In this section, we evaluate NeuralWalker versus several SOTA models on a diverse set of 19 benchmark datasets. We also analyze different components of our model architecture to identify what drives the performance. Appendix D provides more details about the experimental setup, datasets, runtime, and additional results.

Table 1: Test performance on benchmarks from [13]. Metrics with mean \pm std of 4 runs are reported.

	ZINC	MNIST	CIFAR10	PATTERN	CLUSTER
# GRAPHS	12K	70K	60K	14K	12K
AVG. # NODES	23.2	70.6	117.6	118.9	117.2
AVG. # EDGES	24.9	564.5	941.1	3039.3	2150.9
METRIC	MAE \downarrow	ACC \uparrow	ACC \uparrow	ACC \uparrow	ACC \uparrow
GCN [26]	0.367 \pm 0.011	90.705 \pm 0.218	55.710 \pm 0.381	71.892 \pm 0.334	68.498 \pm 0.976
GIN [50]	0.526 \pm 0.051	96.485 \pm 0.252	55.255 \pm 1.527	85.387 \pm 0.136	64.716 \pm 1.553
GAT [47]	0.384 \pm 0.007	95.535 \pm 0.205	64.223 \pm 0.455	78.271 \pm 0.186	70.587 \pm 0.447
GATEDGCN [7]	0.282 \pm 0.015	97.340 \pm 0.143	67.312 \pm 0.311	85.568 \pm 0.088	73.840 \pm 0.326
GRAPHORMER [51]	0.122 \pm 0.006	–	–	–	–
SAT [9]	0.089 \pm 0.002	–	–	86.848 \pm 0.037	77.856 \pm 0.104
GPS [39]	0.070 \pm 0.004	98.051 \pm 0.126	72.298 \pm 0.356	86.685 \pm 0.059	78.016 \pm 0.180
EXPHORMER [41]	–	98.55 \pm 0.03	74.69 \pm 0.13	86.70 \pm 0.03	78.07 \pm 0.037
CRAWL [45]	0.085 \pm 0.004	97.944 \pm 0.050	69.013 \pm 0.259	–	–
NEURALWALKER	0.065 \pm 0.001	98.760 \pm 0.079	80.027 \pm 0.185	86.977 \pm 0.012	78.189 \pm 0.188

Table 2: Test performance on LRGB [15]. Metrics with mean \pm std of 4 runs are reported. NeuralWalker improves the best baseline by 10% and 13% on **PascalVOC-SP** and **COCO-SP** respectively.

	PASCALVOC-SP	COCO-SP	PEPTIDES-FUNC	PEPTIDES-STRUCT	PCQM-CONTACT
# GRAPHS	11.4K	123.3K	15.5K	15.5K	529.4K
AVG. # NODES	479.4	476.9	150.9	150.9	30.1
AVG. # EDGES	2,710.5	2,693.7	307.3	307.3	61.0
METRIC	F1 \uparrow	F1 \uparrow	AP \uparrow	MAE \downarrow	MRR \uparrow
GCN [26, 44]	0.2078 \pm 0.0031	0.1338 \pm 0.0007	0.6860 \pm 0.0050	0.2460 \pm 0.0007	0.4526 \pm 0.0006
GIN [50, 44]	0.2718 \pm 0.0054	0.2125 \pm 0.0009	0.6621 \pm 0.0067	0.2473 \pm 0.0017	0.4617 \pm 0.0005
GATEDGCN [7, 44]	0.3880 \pm 0.0040	0.2922 \pm 0.0018	0.6765 \pm 0.0047	0.2477 \pm 0.0009	0.4670 \pm 0.0004
GPS [39]	0.3748 \pm 0.0109	0.3412 \pm 0.0044	0.6535 \pm 0.0041	0.2500 \pm 0.0005	–
GPS [44]	0.4440 \pm 0.0065	0.3884 \pm 0.0055	0.6534 \pm 0.0091	0.2509 \pm 0.0014	0.4703 \pm 0.0014
EXPHORMER [41]	0.3975 \pm 0.0037	0.3455 \pm 0.0009	0.6527 \pm 0.0043	0.2481 \pm 0.0007	–
CRAWL [45]	–	–	0.7074 \pm 0.0032	0.2506 \pm 0.0022	–
NEURALWALKER	0.4912 \pm 0.0042	0.4398 \pm 0.0033	0.7096 \pm 0.0078	0.2463 \pm 0.0005	0.4707 \pm 0.0007

5.1 Benchmarking NeuralWalker to state-of-the-art methods

We compare NeuralWalker against several popular message passing GNNs, GTs, and walk-based models. GNNs include GCN [26], GIN [50], GAT [47], GatedGCN [7]. GTs include Graphormer [51], GraphTrans [49], SAT [9], GPS [39], Exphormer [41]. Walk-based models include CRaWL [45]. To ensure diverse benchmarking tasks, we use datasets from Benchmarking-GNNs [13], Long-Range Graph Benchmark (LRGB) [15], Open Graph Benchmark (OGB) [22], and node classification datasets from [38, 28].

Benchmarking GNNs. We evaluated NeuralWalker’s performance on five tasks from the Benchmarking GNNs suite: ZINC, MNIST, CIFAR10, PATTERN, and CLUSTER (results in Table 1). Significantly, NeuralWalker achieved SOTA results on all datasets, surpassing all benchmark GNNs and graph transformers (GTs), including the well-tuned and powerful GPS model. Notably, on the CIFAR10 dataset, NeuralWalker outperformed the second-best method by a substantial margin of up to 7% (80.03 vs 74.69). This exceptional performance on CIFAR10, a dataset with directed graphs, suggests that NeuralWalker’s combination of oriented random walks and message passing is particularly adept at capturing the structure of directed graphs. Overall, these results demonstrate NeuralWalker’s strong performance and expressivity across diverse synthetic benchmark tasks.

Long-Range Graph Benchmark. We further evaluated NeuralWalker’s ability to capture long-range dependencies on the recently introduced LRGB benchmark, encompassing five datasets designed to test this very capability (details in [39, 15]). Note that for PCQM-Contact, we used the filtered Mean Reciprocal Rank (MRR), introduced by [44], as the evaluation metric. NeuralWalker consistently outperformed all baseline methods across all but one task (see Table 2). Notably, on datasets like PascalVOC-SP and COCO-SP, where previous work has shown the importance of long-range dependencies (e.g., [44]), NeuralWalker significantly surpassed even SOTA GTs like GPS by a substantial margin, exceeding a 10% improvement.

Table 3: Test performance on OGB [22]. Metrics with mean \pm std of 10 runs are reported.

DATASET	OGBG-MOLPCBA	OGBG-PPA	OGBG-CODE2
# GRAPHS	437.9K	158.1K	452.7K
AVG. # NODES	26.0	243.4	125.2
AVG. # EDGES	28.1	2,266.1	124.2
METRIC	AP \uparrow	ACC \uparrow	F1 \uparrow
GCN [26]	0.2424 \pm 0.0034	0.6857 \pm 0.0061	0.1595 \pm 0.0018
GIN [50]	0.2703 \pm 0.0023	0.7037 \pm 0.0107	0.1581 \pm 0.0026
GRAPHTRANS [49]	0.2761 \pm 0.0029	–	0.1830 \pm 0.0024
SAT [9]	–	0.7522 \pm 0.0056	0.1937 \pm 0.0028
GPS [39]	0.2907 \pm 0.0028	0.8015 \pm 0.0033	0.1894 \pm 0.0024
CRAWL [45]	0.2986 \pm 0.0025	–	–
NEURALWALKER	0.3086 \pm 0.0031	0.7888 \pm 0.0059	0.1957 \pm 0.0025

Table 4: Test performance on node classification benchmarks from [38] and [28]. Metrics with mean \pm std of 10 runs are reported.

DATASET	ROMAN-EMPIRE	AMAZON-RATINGS	MINESWEEPER	TOLOKERS	QUESTIONS	POKEC
# NODES	22,662	24,492	10,000	11,758	48,921	1,632,803
# EDGES	32,927	93,050	39,402	519,000	153,540	30,622,564
METRIC	ACC \uparrow	ACC \uparrow	ROC AUC \uparrow	ROC AUC \uparrow	ROC AUC \uparrow	ACC \uparrow
GCN [26]	73.69 \pm 0.74	48.70 \pm 0.63	89.75 \pm 0.52	83.64 \pm 0.67	76.09 \pm 1.27	75.45 \pm 0.17
GAT(-SEP) [47, 38]	88.75 \pm 0.41	52.70 \pm 0.62	93.91 \pm 0.35	83.78 \pm 0.43	76.79 \pm 0.71	72.23 \pm 0.18
GPS [39]	82.00 \pm 0.61	53.10 \pm 0.42	90.63 \pm 0.67	83.71 \pm 0.48	71.73 \pm 1.47	OOM
NAGPHORMER [10]	74.34 \pm 0.77	51.26 \pm 0.72	84.19 \pm 0.66	78.32 \pm 0.95	68.17 \pm 1.53	76.59 \pm 0.25
EXPHORMER [41]	89.03 \pm 0.37	53.51 \pm 0.46	90.74 \pm 0.53	83.77 \pm 0.78	73.94 \pm 1.06	OOM
POLYNORMER [11]	92.55 \pm 0.37	54.81 \pm 0.49	97.46 \pm 0.36	85.91 \pm 0.74	78.92 \pm 0.89	86.10 \pm 0.05
NEURALWALKER	92.92 \pm 0.36	54.58 \pm 0.36	97.82 \pm 0.40	85.56 \pm 0.74	78.52 \pm 1.13	86.46 \pm 0.09

Open Graph Benchmark. To assess NeuralWalker’s scalability on massive quantities of graphs, we evaluated it on the OGB benchmark, which includes datasets exceeding 100K graphs each. For computational efficiency, we employed 1D CNNs as the sequence layers in this experiment. NeuralWalker achieved SOTA performance on two out of the three datasets (Table 3), demonstrating its ability to handle large-scale graph data. However, the OGBG-PPA dataset presented challenges with overfitting. On this dataset, NeuralWalker with just one block outperformed its multiblock counterpart on this dataset, suggesting potential limitations in regularization needed for specific tasks.

Node classification on large graphs. We further explored NeuralWalker’s ability to handle large graphs in node classification tasks. We integrated NeuralWalker with Polynormer [11], the current SOTA method in this domain. In this experiment, NeuralWalker utilized very long walks (up to 1,000 steps) with a low sampling rate (≤ 0.01) to capture long-range dependencies, instead of using the standard global message-passing step within Polynormer. Despite not using global message passing, NeuralWalker achieved comparable performance to SOTA methods (Table 4), demonstrating its scalability and effectiveness in modeling large graphs. Notably, NeuralWalker can still be efficiently run on the large pokec dataset (1.6M nodes) using a single H100 GPU with 80GB of RAM.

5.2 Ablation studies

Here, we dissect the main components of our model architecture to gauge their contribution to predictive performance and to guide dataset-specific hyperparameter optimization.

We perform ablation studies on three datasets, from small to large graphs. We first demonstrate the importance of combining random walk encoder blocks with local and global message passing blocks. Then, we compare different options for the sequence layer and identify the best choice. Finally, we show the impact of varying the sampling rate and length of the random walks, which can be summarized as a trade-off between expressivity and complexity. This is a unique property of our model compared to MPNNs. All ablation results are performed on the *validation set*, averaged over 4 random seeds, and summarized in Table 5. Since NeuralWalker’s output depends on the sampled random walks at inference, we demonstrate its robustness to sampling variability in Appendix D.4.

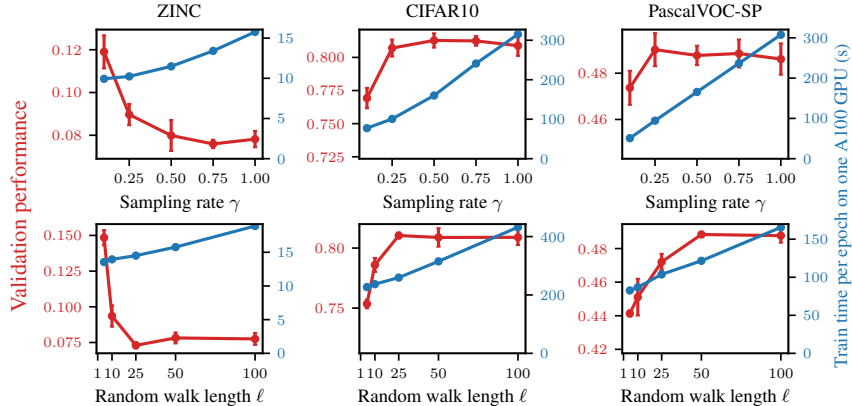


Figure 3: Validation performance when varying sampling rate and length of random walks.

Effect of local & global message passing. Driven by limitations of pure walk-based encoders in efficiently capturing intricate graph relationships [45], this study investigates whether message passing can provide complementary information. We conduct an ablation study (Table 5) to compare NeuralWalker with and without local or global message passing modules. For simplicity, the local module uses GIN with edge features [50, 23]. For global message passing, we explore virtual node layers [19] and transformer layers [46, 9]. Holding the sequence layer fixed, NeuralWalker with message passing consistently outperforms the version without, confirming that random walks and message passing offer complementary strengths. Notably, local message passing consistently improves performance, suggesting its effectiveness in capturing local context and centrality information. The benefit of global message passing, however, varies across datasets. Interestingly, large graphs like PascalVOC-SP show a more significant gain from global message passing. This suggests that future work could combine different local and global message passing techniques or even automatically identify optimal configurations for specific datasets.

Comparison of sequence layer architectures. We analyzed the impact of different sequence layer architectures discussed in Section 3.4 on walk embeddings. These included a CNN, a transformer with rotary position encoding, and SSMs like S4 and Mamba. Surprisingly, transformers underperformed consistently compared to other architectures, in contrast to their high performance in domains like NLP. This could be due to the special sequential nature of walk embeddings, which might not be well-suited for the attention mechanism heavily relied upon by transformers. Further research into domain-specific transformer architectures for walk embeddings presents an intriguing direction.

Mamba emerged as the top performer across datasets, consistently surpassing its predecessor S4. However, CNNs offer a compelling alternative for large datasets due to their significantly faster computation (typically 2-3x faster than Mamba on A100). This presents a practical trade-off: Mamba offers superior accuracy but requires more computational resources. CNNs might be preferable for very large datasets or real-time applications where speed is critical. Notably, the bidirectional Mamba outperformed the original version, particularly on datasets with directed graphs (e.g. CIFAR10). This highlights the importance of capturing information flow in both directions on directed graphs.

Impact of random walk sampling strategies. We investigated how varying the sampling rate and length of random walks affects NeuralWalker’s performance, particularly when using Mamba as the sequence layer. Note that we only vary the sampling rate at training, the sampling rate at inference is fixed at 1.0 to maximize the coverage. As expected, a larger number of longer walks leads to broader coverage of the graph’s structure, leading to a clear performance boost according to Figure 3. However, this improvement plateaus as walks become sufficiently long, suggesting diminishing returns beyond a certain point. Importantly, this gain in performance comes at the cost of increased computation time, which scales linearly with both sampling rate and walk length, as predicted by the complexity of Mamba [20]. This highlights the trade-off between expressivity and complexity, which could be explicitly controlled by these two hyperparameters. Future work could explore more efficient sampling strategies to minimize the necessary sampling rate, potentially investigating techniques like importance sampling or adaptive walk lengths based on graph properties.

Table 5: Ablation studies of NeuralWalker on different choices of the sequence layer type, local and global message passing. Validation performances with mean \pm std of 4 runs are reported. We compare different choices of sequence layers (Mamba, S4, CNN, and Transformer), local (with or without GIN) and global (virtual node (VN), Transformer, or none (w/o)) message passing layers.

SEQUENCE LAYER	LOCAL MP	GLOBAL MP	ZINC	CIFAR10	PASCALVOC-SP
MAMBA	GIN	VN	0.078 \pm 0.004	78.610 \pm 0.524	0.4672 \pm 0.0077
MAMBA	GIN	TRANS.	0.083 \pm 0.003	80.755 \pm 0.467	0.4877 \pm 0.0042
MAMBA	GIN	w/o	0.085 \pm 0.003	80.885 \pm 0.769	0.4611 \pm 0.0036
MAMBA	w/o	VN	0.086 \pm 0.008	78.025 \pm 0.552	0.4570 \pm 0.0064
MAMBA	w/o	w/o	0.090 \pm 0.002	79.035 \pm 0.850	0.4525 \pm 0.0044
MAMBA (w/o BID)	GIN	VN	0.089 \pm 0.004	74.910 \pm 0.547	0.4522 \pm 0.0063
S4	GIN	VN	0.082 \pm 0.004	77.970 \pm 0.506	0.4559 \pm 0.0064
CNN	GIN	VN	0.088 \pm 0.004	80.240 \pm 0.767	0.4652 \pm 0.0058
CNN	GIN	TRANS.	0.092 \pm 0.004	80.665 \pm 0.408	0.4790 \pm 0.0081
CNN	GIN	w/o	0.102 \pm 0.003	80.020 \pm 0.279	0.4155 \pm 0.0050
TRANS.	GIN	VN	0.084 \pm 0.003	72.850 \pm 0.373	0.4316 \pm 0.0072

In practice, this necessitates careful consideration of resource constraints when selecting the sampling rate and walk length to achieve the best performance within time and budget limitations.

6 Conclusion

We have introduced NeuralWalker, a powerful and flexible architecture that combines random walks and message passing to address the expressivity limitations of structural encoding in graph learning. By treating random walks as sequences and leveraging advanced sequence modeling techniques, NeuralWalker achieves superior performance compared to existing GNNs and GTs, as demonstrated through extensive experimentation on various benchmarks. Looking forward, we acknowledge opportunities for further exploration. First, investigating more efficient random walk sampling strategies with improved graph coverage could potentially enhance NeuralWalker’s performance. Second, exploring self-supervised learning techniques for walk sequences holds promise for extending NeuralWalker’s applicability to unlabeled graphs.

Limitations. NeuralWalker demonstrates good scalability to large graphs. However, one potential limitation lies in the trade-off between the sampling efficiency of random walks and graph coverage for very large graphs. In this work, we explored a computationally efficient sampling strategy but probably not with the optimal graph coverage. Investigating more efficient random walk sampling strategies that improve coverage while maintaining computational efficiency could further enhance NeuralWalker’s performance.

Additionally, we identify a scarcity of publicly available graph datasets with well-defined long-range dependencies. While datasets like LRGB provide valuable examples, the limited number of such datasets hinders comprehensive evaluation and the potential to push the boundaries of long-range dependency capture in graph learning tasks. Furthermore, based on our experiments and [44], only 2 out of the 5 datasets in LRGB seem to present long-range dependencies.

Broader impacts While our research primarily focuses on general graph representation learning, we recognize the importance of responsible and ethical application in specialized fields. When utilized in domains such as drug discovery or computational biology, careful attention must be paid to ensuring the trustworthiness and appropriate use of our method to mitigate potential misuse. Our extensive experiments demonstrate the significant potential of our approach in both social network and biological network analysis, highlighting the promising societal benefits our work may offer in these specific areas.

Acknowledgements

We thank Luis Wyss and Trenton Chang for their insightful feedback on the manuscript.

References

- [1] R. Aleliunas, R. M. Karp, R. J. Lipton, L. Lovász, and C. Rackoff. Random walks, universal traversal sequences, and the complexity of maze problems. In *Symposium on Foundations of Computer Science (SFCS)*, 1979.
- [2] U. Alon and E. Yahav. On the bottleneck of graph neural networks and its practical implications. In *International Conference on Learning Representations (ICLR)*, 2021.
- [3] P. Barceló, E. V. Kostylev, M. Monet, J. Pérez, J. Reutter, and J.-P. Silva. The logical expressiveness of graph neural networks. In *International Conference on Learning Representations (ICLR)*, 2020.
- [4] A. Behrouz and F. Hashemi. Graph mamba: Towards learning on graphs with state space models. *arXiv preprint arXiv:2402.08678*, 2024.
- [5] K. M. Borgwardt and H.-P. Kriegel. Shortest-path kernels on graphs. In *International conference on data mining (ICDM)*, 2005.
- [6] G. Bouritsas, F. Frasca, S. Zafeiriou, and M. M. Bronstein. Improving graph neural network expressivity via subgraph isomorphism counting. *IEEE Trans. Pattern Anal. Mach. Intell.*, 45(1):657–668, 2023.
- [7] X. Bresson and T. Laurent. Residual gated graph convnets. *arXiv preprint arXiv:1711.07553*, 2017.
- [8] D. Chen, L. Jacob, and J. Mairal. Convolutional kernel networks for graph-structured data. In *International Conference on Machine Learning (ICML)*, 2020.
- [9] D. Chen, L. O’Bray, and K. Borgwardt. Structure-aware transformer for graph representation learning. In *International Conference on Machine Learning (ICML)*, 2022.
- [10] J. Chen, K. Gao, G. Li, and K. He. Nagphormer: A tokenized graph transformer for node classification in large graphs. In *International Conference on Learning Representations (ICLR)*, 2022.
- [11] C. Deng, Z. Yue, and Z. Zhang. Polynormer: Polynomial-expressive graph transformer in linear time. In *International Conference on Learning Representations (ICLR)*, 2024.
- [12] R. M. Dudley. *Real analysis and probability*. Cambridge University Press, 2018.
- [13] V. P. Dwivedi, C. K. Joshi, A. T. Luu, T. Laurent, Y. Bengio, and X. Bresson. Benchmarking graph neural networks. *Journal of Machine Learning Research*, 24(43):1–48, 2023.
- [14] V. P. Dwivedi, A. T. Luu, T. Laurent, Y. Bengio, and X. Bresson. Graph neural networks with learnable structural and positional representations. In *International Conference on Learning Representations (ICLR)*, 2021.
- [15] V. P. Dwivedi, L. Rampášek, M. Galkin, A. Parviz, G. Wolf, A. T. Luu, and D. Beaini. Long range graph benchmark. In *Advances in Neural Information Processing Systems (NeurIPS)*, 2022.
- [16] W. Fan, Y. Ma, Q. Li, Y. He, E. Zhao, J. Tang, and D. Yin. Graph neural networks for social recommendation. In *The World Wide Web Conference*, 2019.
- [17] M. Fey and J. E. Lenssen. Fast graph representation learning with PyTorch Geometric. In *ICLR Workshop on Representation Learning on Graphs and Manifolds*, 2019.
- [18] T. Gärtner, P. Flach, and S. Wrobel. On graph kernels: Hardness results and efficient alternatives. In *COLT*. Springer, 2003.
- [19] J. Gilmer, S. S. Schoenholz, P. F. Riley, O. Vinyals, and G. E. Dahl. Neural message passing for quantum chemistry. In *International Conference on Machine Learning (ICML)*, 2017.
- [20] A. Gu and T. Dao. Mamba: Linear-time sequence modeling with selective state spaces. *arXiv preprint arXiv:2312.00752*, 2023.
- [21] A. Gu, K. Goel, and C. Re. Efficiently modeling long sequences with structured state spaces. In *International Conference on Learning Representations (ICLR)*, 2021.
- [22] W. Hu, M. Fey, M. Zitnik, Y. Dong, H. Ren, B. Liu, M. Catasta, and J. Leskovec. Open Graph Benchmark: Datasets for Machine Learning on Graphs. In *Advances in Neural Information Processing Systems (NeurIPS)*, 2020.

- [23] W. Hu, B. Liu, J. Gomes, M. Zitnik, P. Liang, V. Pande, and J. Leskovec. Strategies for pre-training graph neural networks. In *International Conference on Learning Representations (ICLR)*, 2019.
- [24] J. Ingraham, V. Garg, R. Barzilay, and T. Jaakkola. Generative models for graph-based protein design. In *Advances in Neural Information Processing Systems (NeurIPS)*, 2019.
- [25] H. Kashima, K. Tsuda, and A. Inokuchi. Marginalized kernels between labeled graphs. In *International Conference on Machine Learning (ICML)*, 2003.
- [26] T. N. Kipf and M. Welling. Semi-supervised classification with graph convolutional networks. In *International Conference on Learning Representations (ICLR)*, 2016.
- [27] D. Kreuzer, D. Beaini, W. Hamilton, V. Létourneau, and P. Tossou. Rethinking graph transformers with spectral attention. In *Advances in Neural Information Processing Systems (NeurIPS)*, 2021.
- [28] J. Leskovec and A. Krevl. SNAP Datasets: Stanford large network dataset collection. <http://snap.stanford.edu/data>, June 2014.
- [29] D. Lim, F. Hohne, X. Li, S. L. Huang, V. Gupta, O. Bhalerao, and S. N. Lim. Large scale learning on non-homophilous graphs: New benchmarks and strong simple methods. In *Advances in Neural Information Processing Systems (NeurIPS)*, 2021.
- [30] L. Lovász. Random walks on graphs. *Combinatorics, Paul erdos is eighty*, 2(1-46):4, 1993.
- [31] P. Mahé, N. Ueda, T. Akutsu, J.-L. Perret, and J.-P. Vert. Graph kernels for molecular structure-activity relationship analysis with support vector machines. *Journal of chemical information and modeling*, 45(4):939–951, 2005.
- [32] G. Mialon, D. Chen, M. Selosse, and J. Mairal. Graphit: Encoding graph structure in transformers. *arXiv preprint arXiv:2106.05667*, 2021.
- [33] G. Michel, G. Nikolentzos, J. F. Lutzeyer, and M. Vazirgiannis. Path neural networks: Expressive and accurate graph neural networks. In *International Conference on Machine Learning (ICML)*, 2023.
- [34] A. Müller. Integral probability metrics and their generating classes of functions. *Advances in applied probability*, 29(2):429–443, 1997.
- [35] G. Nikolentzos and M. Vazirgiannis. Random walk graph neural networks. In *Advances in Neural Information Processing Systems (NeurIPS)*, 2020.
- [36] K. Oono and T. Suzuki. Graph neural networks exponentially lose expressive power for node classification. In *International Conference on Learning Representations (ICLR)*, 2020.
- [37] J. Pata, J. Duarte, J.-R. Vlimant, M. Pierini, and M. Spiropulu. Mlpf: efficient machine-learned particle-flow reconstruction using graph neural networks. *The European Physical Journal C*, 81:1–14, 2021.
- [38] O. Platonov, D. Kuznedelev, M. Diskin, A. Babenko, and L. Prokhorenkova. A critical look at the evaluation of gnns under heterophily: Are we really making progress? In *International Conference on Learning Representations (ICLR)*, 2022.
- [39] L. Rampášek, M. Galkin, V. P. Dwivedi, A. T. Luu, G. Wolf, and D. Beaini. Recipe for a general, powerful, scalable graph transformer. *Advances in Neural Information Processing Systems (NeurIPS)*, 2022.
- [40] A. Sanchez-Gonzalez, J. Godwin, T. Pfaff, R. Ying, J. Leskovec, and P. Battaglia. Learning to simulate complex physics with graph networks. In *International Conference on Machine Learning (ICML)*, 2020.
- [41] H. Shirzad, A. Vellingker, B. Venkatachalam, D. J. Sutherland, and A. K. Sinop. Exphormer: Sparse transformers for graphs. In *International Conference on Machine Learning (ICML)*, 2023.
- [42] J. M. Stokes, K. Yang, K. Swanson, W. Jin, A. Cubillos-Ruiz, N. M. Donghia, C. R. MacNair, S. French, L. A. Carfrae, Z. Bloom-Ackermann, et al. A deep learning approach to antibiotic discovery. *Cell*, 180(4):688–702, 2020.
- [43] J. Su, M. Ahmed, Y. Lu, S. Pan, W. Bo, and Y. Liu. Roforner: Enhanced transformer with rotary position embedding. *Neurocomputing*, 568:127063, 2024.

- [44] J. Tönshoff, M. Ritzert, E. Rosenbluth, and M. Grohe. Where did the gap go? reassessing the long-range graph benchmark. In *Learning on Graphs Conference*, 2023.
- [45] J. Tönshoff, M. Ritzert, H. Wolf, and M. Grohe. Walking out of the weisfeiler leman hierarchy: Graph learning beyond message passing. *Transactions on Machine Learning Research (TMLR)*, 2023.
- [46] A. Vaswani, N. Shazeer, N. Parmar, J. Uszkoreit, L. Jones, A. N. Gomez, Ł. Kaiser, and I. Polosukhin. Attention is all you need. In *Advances in Neural Information Processing Systems (NeurIPS)*, 2017.
- [47] P. Veličković, G. Cucurull, A. Casanova, A. Romero, P. Liò, and Y. Bengio. Graph attention networks. In *International Conference on Learning Representations (ICLR)*, 2018.
- [48] C. Wang, O. Tsepa, J. Ma, and B. Wang. Graph-mamba: Towards long-range graph sequence modeling with selective state spaces. *arXiv preprint arXiv:2402.00789*, 2024.
- [49] Z. Wu, P. Jain, M. Wright, A. Mirhoseini, J. E. Gonzalez, and I. Stoica. Representing long-range context for graph neural networks with global attention. In *Advances in Neural Information Processing Systems (NeurIPS)*, 2021.
- [50] K. Xu, W. Hu, J. Leskovec, and S. Jegelka. How powerful are graph neural networks? In *International Conference on Learning Representations (ICLR)*, 2019.
- [51] C. Ying, T. Cai, S. Luo, S. Zheng, G. Ke, D. He, Y. Shen, and T.-Y. Liu. Do transformers really perform badly for graph representation? In *Advances in Neural Information Processing Systems (NeurIPS)*, 2021.
- [52] L. Zhu, B. Liao, Q. Zhang, X. Wang, W. Liu, and X. Wang. Vision mamba: Efficient visual representation learning with bidirectional state space model. *arXiv preprint arXiv:2401.09417*, 2024.
- [53] W. Zhu, T. Wen, G. Song, L. Wang, and B. Zheng. On structural expressive power of graph transformers. In *Conference on Knowledge Discovery and Data Mining (KDD)*, 2023.

Appendix

This appendix provides both theoretical and experimental materials and is organized as follows: Section A provides a more detailed background of related work. Section B presents some additional remarks on Neural Walker, including limitations and societal impacts. Section C provides theoretical background and proofs. Section D provides experimental details and additional results.

A Background

A.1 Message-Passing Graph Neural Networks

Graph Neural Networks (GNNs) refine node representations iteratively by integrating information from neighboring nodes. Xu et al. (2019) [50] provide a unifying framework for this process, consisting of three key steps: AGGREGATE, COMBINE, and READOUT. Various GNN architectures can be seen as variations within these functions.

In each layer, the AGGREGATE step combines representations from neighboring nodes (e.g., using sum or mean), which are then merged with the node’s previous representation in the COMBINE step. This is typically followed by a non-linear activation function, such as ReLU. The updated representations are then passed to the next layer, and this process repeats for each layer in the network. These steps primarily capture local sub-structures, necessitating a deep network to model interactions across the entire graph.

The READOUT function ultimately aggregates node representations to the desired output granularity, whether at the node or graph level. Both AGGREGATE and READOUT steps must be permutation invariant. This framework offers a comprehensive perspective for understanding the diverse array of GNN architectures.

A.2 Transformer on Graphs

While Graph Neural Networks (GNNs) explicitly utilize graph structures, Transformers infer node relationships by focusing on node attributes. Transformers, introduced by [46], treat the graph as a (multi-)set of nodes and use self-attention to determine node similarity.

A Transformer consists of two main components: a self-attention module and a feed-forward neural network (FFN). In self-attention, input features \mathbf{X} are linearly projected into query (\mathbf{Q}), key (\mathbf{K}), and value (\mathbf{V}) matrices. Self-attention is then computed as:

$$\text{Attn}(\mathbf{X}) := \text{softmax} \left(\frac{\mathbf{Q}\mathbf{K}^T}{\sqrt{d_{\text{out}}}} \right) \mathbf{V} \in \mathbb{R}^{n \times d_{\text{out}}},$$

where d_{out} is the dimension of \mathbf{Q} . Multi-head attention, which concatenates multiple instances of this equation, has proven effective in practice.

A Transformer layer combines self-attention with a skip connection and FFN:

$$\begin{aligned} \mathbf{X}' &= \mathbf{X} + \text{Attn}(\mathbf{X}), \\ \mathbf{X}'' &= \text{FFN}(\mathbf{X}') := \text{ReLU}(\mathbf{X}'W_1)W_2. \end{aligned}$$

Stacking multiple layers forms a Transformer model, resulting in node-level representations. However, due to self-attention’s permutation equivariance, Transformers produce identical representations for nodes with matching attributes, regardless of their graph context. Thus, incorporating structural information, typically through positional or structural encoding such as Laplacian positional encoding or random walk structural encoding [14, 39], is crucial.

A.3 State Space Models

As we treat random walks explicitly as sequences, recent advances in long sequence modeling could be leveraged directly to model random walks. SSMs are a type of these models that have shown

promising performance in long sequence modeling. SSMs map input sequence $x(t) \in \mathbb{R}$ to some response sequence $y(t) \in \mathbb{R}$ through an implicit state $h(t) \in \mathbb{R}^N$ and three parameters (A, B, C) :

$$h'(t) = Ah(t) + Bx(t), \quad y(t) = Ch(t).$$

For computational reasons, structured SSMs (S4) [21] proposes to discretize the above system by introducing a time step variable Δ and a discretization rule, leading to a reparametrization of the parameters A and B . Then, the discrete-time SSMs can be computed in two ways either as a linear recurrence or a global convolution. Recently, a selection mechanism [20] has been introduced to control which part of the sequence can flow into the hidden states, making the parameters in SSMs time and data-dependent. The proposed model, named Mamba, significantly outperforms its predecessors and results in several successful applications in many tasks. More recently, a bidirectional version of Mamba [52] has been proposed to handle image data, by averaging the representations of both forward and backward sequences after each Mamba block.

B Additional Remarks on Neural Walker

B.1 Illustration of the Position Encodings for Random Walks

Here, we give a visual example of the positional encodings that we presented in Section 3.2. The example is shown in Figure 4.

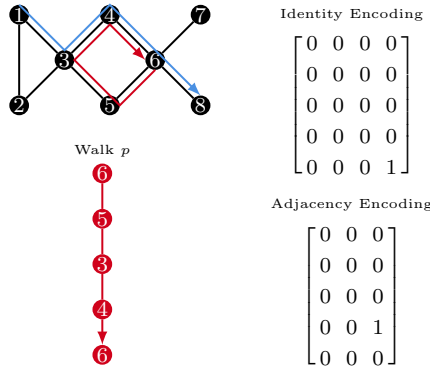


Figure 4: An example of the identity encoding and adjacency encoding presented in Section 3.2. On the random walk colored in red, we have $\text{id}_W[4, 3] = 1$ as $w_4 = w_0 = 6$. We have $\text{adj}_W[3, 2] = 1$ as $w_3w_0 \in E$ is an edge of the graph.

C Theoretical Results

In this section, we give more background of random walks on graphs and present the theoretical properties of NeuralWalker.

C.1 Stability Results

Definition C.1 (Walk feature vector). *For any graph $G = (V, E, x, z)$ and $W \in \mathcal{W}_\ell(G)$, the walk feature vector X_W of W is defined, by concatenating the node and edge feature vectors as well as the positional encodings along W of window size $s = \ell$, as*

$$X_W = (x(w_i), z(w_iw_{i+1}), h_{pe}[i])_{i=0, \dots, \ell} \in \mathbb{R}^{(\ell+1) \times d_{\text{walk}}},$$

where h_{pe} is the positional encoding in Section 3.2, $\mathbf{z}_{w_\ell w_{\ell+1}} = 0$, and $d_{\text{walk}} := d + d' + d_{pe}$. By abuse of notation, we denote by $P(\mathcal{W}(G))$ any distribution of walk feature vectors on G .

Lemma C.2. *The walk feature vector with full graph coverage uniquely determines the graph, i.e., for two graphs G and G' in \mathcal{G}_n if there exists a walk $W \in \mathcal{W}_\ell(G)$ visiting all nodes on G and a walk $W' \in \mathcal{W}_\ell$ visiting all nodes on G' such that $X_W = X_{W'}$, then G and G' are isomorphic.*

Proof. The proof is immediate following the Observation 1 of [45]. □

Now if we replace the normalization factor $N_v(P_m(\mathcal{W}_\ell(G)))$ in the walk aggregator in Section 3.5 with a simpler deterministic constant $m\ell/|V|$ and apply an average pooling followed by a linear layer $x \mapsto u^\top x + b \in \mathbb{R}$ to the output of the walk aggregator, then the resulting function $g_{f,m,\ell} : \mathcal{G} \rightarrow \mathbb{R}$ defined on the graph space \mathcal{G} can be rewritten as the average of some function of walk feature vectors:

$$g_{f,m,\ell}(G) = \frac{1}{m} \sum_{W \in P_m(\mathcal{W}_\ell(G))} f(X_W), \quad (9)$$

where

$$f(X_W) = \frac{1}{\ell} \sum_{w_i \in W} (u^\top f_{seq}(h_W)[i] + b), \quad (10)$$

and h_W defined in Eq. (1) depend on X_W .

Note that the above replacement of the normalization factor is not a strong assumption. It is based on the following lemmas:

Lemma C.3 ([30]). *Let G be a connected graph. For a random walk $W \sim P(\mathcal{W}(G))$ with $W = (w_0, w_1, \dots, w_t, \dots)$, we denote by P_t the distribution of w_t . Then,*

$$\pi(v) = \frac{d(v)}{2|E|},$$

where $d(v)$ denotes the degree of node v , is the (unique) stationary distribution, i.e., if $P_0 = \pi$ then $P_t = P_0$ for any t . If $P_0 = \pi(v)$, then we have

$$\mathbb{E}[N_v(P_m(\mathcal{W}_\ell(G)))] = \frac{m\ell d(v)}{2|E|}.$$

In particular, if G is a regular graph, $\pi(v) = 1/|V|$ is the uniform distribution and $\mathbb{E}[N_v(P_m(\mathcal{W}_\ell(G)))] = m\ell/|V|$.

Lemma C.4 ([30]). *If G is a non-bipartite graph, then $P_t \rightarrow \pi(v)$ as $t \rightarrow \infty$.*

The above two lemmas link the random normalization factor to the deterministic one.

If we have a sufficiently large number of random walks, by the law of large numbers, we have

$$g_{f,m,\ell}(G) \xrightarrow{a.s.} g_{f,\ell} := \mathbb{E}_{X_W \sim P(\mathcal{W}_\ell(G))}[f(X_W)], \quad (11)$$

where $\xrightarrow{a.s.}$ denotes the almost sure convergence. This observation inspires us to consider the following integral probability metric [34] comparing distributions of walk feature vectors:

$$d_{\mathcal{F},\ell}(G, G') := \sup_{f \in \mathcal{F}} |\mathbb{E}_{X_W \sim P(\mathcal{W}_\ell(G))}[f(X_W)] - \mathbb{E}_{X_{W'} \sim P(\mathcal{W}_\ell(G'))}[f(X_{W'})]|, \quad (12)$$

where \mathcal{F} is some functional class, such as the class of neural networks defined by the NeuralWalker model. This is actually a metric on the graph space \mathcal{G}_n of bounded order n if \mathcal{F} is universal space:

Theorem C.5. *If \mathcal{F} is a universal space and $\ell \geq 4n^3$, then $d_{\mathcal{F},\ell} : \mathcal{G} \times \mathcal{G} \rightarrow \mathbb{R}_+$ is a metric on \mathcal{G}_n satisfying:*

- (positivity) if G and G' are non-isomorphic, then $d_{\mathcal{F}}(G, G') > 0$.
- (symmetry) $d_{\mathcal{F}}(G, G') = d_{\mathcal{F}}(G', G)$.
- (triangle inequality) $d_{\mathcal{F}}(G, G'') \leq d_{\mathcal{F}}(G, G') + d_{\mathcal{F}}(G', G'')$.

Proof. The symmetry and triangle inequality are trivial by definition of $d_{\mathcal{F},\ell}$. Let us focus on the positivity. We assume that $d_{\mathcal{F},\ell}(G, G') = 0$. By the universality of \mathcal{F} , for any $\varepsilon > 0$ and $f \in C(\mathbb{R}^{d_{\text{walk}}})$, the space of bounded continuous functions on $\mathbb{R}^{d_{\text{walk}}}$, there exists a $g \in \mathcal{F}$ such that

$$\|f - g\|_\infty \leq \varepsilon.$$

We then make the expansion

$$\begin{aligned} & |\mathbb{E}_{X_W \sim P(\mathcal{W}_\ell(G))}[f(X_W)] - \mathbb{E}_{X_{W'} \sim P(\mathcal{W}_\ell(G'))}[f(X_{W'})]| \leq \\ & \quad |\mathbb{E}_{X_W \sim P(\mathcal{W}_\ell(G))}[f(X_W)] - \mathbb{E}_{X_W \sim P(\mathcal{W}_\ell(G))}[g(X_W)]| + \\ & \quad |\mathbb{E}_{X_W \sim P(\mathcal{W}_\ell(G))}[g(X_W)] - \mathbb{E}_{X_{W'} \sim P(\mathcal{W}_\ell(G'))}[g(X_{W'})]| + \\ & \quad |\mathbb{E}_{X_{W'} \sim P(\mathcal{W}_\ell(G'))}[g(X_{W'})] - \mathbb{E}_{X_{W'} \sim P(\mathcal{W}_\ell(G'))}[f(X_{W'})]|. \end{aligned}$$

The first and third terms satisfy

$$|\mathbb{E}_{X_W \sim P(\mathcal{W}_\ell(G))}[f(X_W)] - \mathbb{E}_{X_W \sim P(\mathcal{W}_\ell(G))}[g(X_W)]| \leq \mathbb{E}_{X_W \sim P(\mathcal{W}_\ell(G))} |f(X_W) - g(X_W)| \leq \varepsilon,$$

and the second term equals 0 by assumption. Hence,

$$|\mathbb{E}_{X_W \sim P(\mathcal{W}_\ell(G))}[f(X_W)] - \mathbb{E}_{X_{W'} \sim P(\mathcal{W}_\ell(G'))}[f(X_{W'})]| \leq 2\varepsilon,$$

for all $f \in C(\mathbb{R}^{d_{\text{walk}}})$ and $\varepsilon > 0$. This implies $P(\mathcal{W}_\ell(G)) = P(\mathcal{W}_\ell(G'))$ by Lemma 9.3.2 of [12], meaning that the distribution of walk feature vectors of length ℓ in G is identical to the distribution in G' . Without loss of generality, we assume that G and G' are connected and our arguments can be easily generalized to each connected component if G is not connected. Now for a random walk $W \sim P(\mathcal{W}(G))$, let us denote by T_W the number of steps to reach every node on the graph. Then $\mathbb{E}[T_W]$ is called the cover time. A well-known result in graph theory [1] states that the cover time is upper bounded:

$$\mathbb{E}[T_W] \leq 4|V||E|.$$

Therefore the cover time for graphs in \mathcal{G}_n is uniformly bounded by $\mathbb{E}[T_W] \leq 4n^3$ as $|V| \leq n$ and $|E| \leq n^2$. Then, by applying Markov's inequality, we have

$$\mathbb{P}[T_W < 4n^3 + \epsilon] = 1 - \mathbb{P}[T_W \geq 4n^3 + \epsilon] \geq 1 - \frac{\mathbb{E}[T_W]}{4n^3 + \epsilon} \geq \frac{\epsilon}{4n^3 + \epsilon} > 0,$$

for any $\epsilon > 0$. Thus, $\mathbb{P}[T_W \leq 4n^3] > 0$ which means that there exists a random walk of not greater than $4n^3$ that visits all nodes in G . As a result, there exists a random walk of length ℓ reaching all nodes for $\ell \geq 4n^3$. $P(\mathcal{W}_\ell(G)) = P(\mathcal{W}_\ell(G'))$ implies that there also exists a random walk W' in G' such that $X_W = X_{W'}$. As a consequence, G and G' are isomorphic following Lemma C.2. \square

Now that we have a metric space $(\mathcal{G}_n, d_{\mathcal{F}, \ell})$ with $\ell \geq 4n^3$, we can show some useful properties of $g_{f, \ell}$:

Theorem C.6 (Lipschitz continuity of $g_{f, \ell}$). *For any G and G' in \mathcal{G}_n , if \mathcal{F} is a functional space containing f , we have*

$$|g_{f, \ell}(G) - g_{f, \ell}(G')| \leq d_{\mathcal{F}, \ell}(G, G'). \quad (13)$$

Proof. The proof is immediate from the definition of $d_{\mathcal{F}, \ell}$. \square

The Lipschitz property is needed for stability to perturbations in the sense that if G' is close to G in $(\mathcal{G}_n, d_{\mathcal{F}, \ell})$, then their images by $g_{f, \ell}$ (output of the model) are also close.

The following result provides us insight into the rate of convergence of $g_{f, m, \ell}$ to $g_{f, \ell}$:

Theorem C.7 (Convergence rate). *Assume that $\text{Var}[f(X_W)] = \sigma^2 < \infty$. Then, as m tends to infinity, we have*

$$\sqrt{m}(g_{f, m, \ell}(G) - g_{f, \ell}(G)) \xrightarrow{d} \mathcal{N}(0, \sigma^2),$$

where \xrightarrow{d} denotes the convergence in distribution.

Proof. The proof follows the central limit theorem [12]. \square

C.2 Expressivity Results

Theorem C.8 (Injectivity of $g_{f, \ell}$). *Assume \mathcal{F} is a universal space. If G and G' are non-isomorphic graphs, then there exists a $f \in \mathcal{F}$ such that $g_{f, \ell}(G) \neq g_{f, \ell}(G')$ if $\ell \geq 4 \max\{|V|, |V'|\}^3$.*

Proof. We can prove this by contrapositive. We note that $G, G' \in \mathcal{G}_{n_{\max}}$ with $n_{\max} := \max\{|V|, |V'|\}$. Assume that for all $f \in \mathcal{F}$, $g_{f, \ell}(G) = g_{f, \ell}(G')$. This implies that $d_{\mathcal{F}, \ell}(G, G') = 0$. Then by the positivity of $d_{\mathcal{F}, \ell}$ in $\mathcal{G}_{n_{\max}}$, G and G' are isomorphic. \square

The injectivity property ensures that our model with a sufficiently large number of sufficiently long ($\geq 4n^3$) random walks can distinguish between non-isomorphic graphs, highlighting its expressive power.

Complementary to the above results, we now show that the expressive power of our model exceeds that of ordinary message passing neural networks even when considering random walks of small size. We base the following theorem on NeuralWalker's ability to count substructures.

Theorem C.9. For any $\ell \geq 2$, NeuralWalker equipped with the complete walk set \mathcal{W}_ℓ is strictly more expressive than 1-WL, and thus ordinary MPNNs.

In order to prove the above theorem, we first state a result on the expressive power of the walk aggregator function. Roughly speaking, we show that there exist aggregation functions such that for a node v this function counts the number of induced subgraphs that v is part of. Since v assumes a particular role (also referred to as orbit) in the subgraph, we are essentially interested in the subgraph rooted at v . In the following, let G_v denote the graph G rooted at node v and let \simeq denote the isomorphism relation. We now define the set $x_\ell(G, v) = \{\{H \simeq G_v = G[\{w_0, \dots, w_k = v\}], W = (w_0, \dots, w_\ell), W \in \mathcal{W}_\ell(G)\}$ which corresponds to the set of subgraphs with root v that are identified when using random walks of size ℓ .

Lemma C.10. There exists a function h_{agg}^V such that for any node $v \in G, v' \in G'$ and walk length ℓ , it holds that $h_{\text{agg}}^V(v) = h_{\text{agg}}^V(v')$ if and only if $x_\ell(G, v) = x_\ell(G', v')$.

Proof. For simplicity, we assume graphs to be unlabeled, by noting that a generalization to the labeled case requires only slight modifications. Recall that the positional encoding of a walk W encodes the pairwise adjacency of nodes contained in W . In fact, this encoding contains the complete information on the subgraph induced by W . More formally, for a length- ℓ walk $W \in \mathcal{W}_\ell(G)$, the k -th row of the corresponding walk feature vector X_W encodes the induced subgraph $G[\{w_0, \dots, w_k\}]$. Assuming $w_k = v$, we can also infer about the structural role of v in $G[\{w_0, \dots, w_k\}]$. Now, the function h_{agg}^V aggregates this induced subgraph information for sets of subgraphs into node embeddings. That is, for a node $v \in G$ and the set of walks $\mathcal{W}_\ell(G)$, the function $h_{\text{agg}}^V(v)$ maps v to an embedding that aggregates the set $\{\{G_v = G[\{w_0, \dots, w_k = v\}], W = (w_0, \dots, w_\ell), W \in \mathcal{W}_\ell(G)\}$. By considering the complete set of walks $\mathcal{W}_\ell(G)$, we guarantee a deterministic embedding. Assuming a sufficiently powerful neural network, it is easy to see that such a function h_{agg}^V can be realized by our model. The claim immediately follows. \square

By using an aggregation function that fulfils Lemma C.10, the resulting node embeddings encode the set of induced subgraphs that the nodes are part of. For example, with walk length $\ell = 2$, the node embeddings contain the information about the number of triangles that they are part of. In the subsequent message passing step, NeuralWalker propagates this subgraph information. Analogously to e.g. [6], it can easily be shown that with a sufficient number of such message passing layers and a powerful readout network, the resulting graph representations are strictly more powerful than ordinary MPNNs, proving Thm. C.9 above.

D Experimental Details and Additional Results

In this section, we provide implementation details and additional experimental results

D.1 Dataset Description

We provide details of the datasets used in our experiments. For each dataset, we follow their respective training protocols and use the standard train/validation/test splits and evaluation metrics.

ZINC (MIT License) [13]. The ZINC dataset is a subset of the ZINC database, containing 12,000 molecular graphs representing commercially available chemical compounds. These graphs range from 9 to 37 nodes in size, with each node corresponding to a "heavy atom" (one of 28 possible types) and each edge representing a bond (one of 3 types). The goal is to predict the constrained solubility (logP) using regression. The dataset is conveniently pre-split for training, validation, and testing, with a standard split of 10,000/1,000/1,000 molecules for each set, respectively.

MNIST and CIFAR10 (CC BY-SA 3.0 and MIT License) [13]. MNIST and CIFAR10 are adapted for graph-based learning by converting each image into a graph. This is achieved by segmenting the image into superpixels using SLIC (Simple Linear Iterative Clustering) and then connecting each superpixel to its 8 nearest neighbors. The resulting graphs maintain the original 10-class classification task and standard dataset splits (*i.e.*, 55K/5K/10K train/validation/test for MNIST and 45K/5K/10K for CIFAR10.).

Table 6: Summary of the datasets [13, 15, 22] used in this study.

DATASET	# GRAPHS	AVG. # NODES	AVG. # EDGES	DIRECTED	PREDICTION LEVEL	PREDICTION TASK	METRIC
ZINC	12,000	23.2	24.9	No	GRAPH	REGRESSION	MEAN ABS. ERROR
MNIST	70,000	70.6	564.5	YES	GRAPH	10-CLASS CLASSIF.	ACCURACY
CIFAR10	60,000	117.6	941.1	YES	GRAPH	10-CLASS CLASSIF.	ACCURACY
PATTERN	14,000	118.9	3,039.3	No	INDUCTIVE NODE	BINARY CLASSIF.	ACCURACY
CLUSTER	12,000	117.2	2,150.9	No	INDUCTIVE NODE	6-CLASS CLASSIF.	ACCURACY
PASCALVOC-SP	11,355	479.4	2,710.5	No	INDUCTIVE NODE	21-CLASS CLASSIF.	F1 SCORE
COCO-SP	123,286	476.9	2,693.7	No	INDUCTIVE NODE	81-CLASS CLASSIF.	F1 SCORE
PEPTIDES-FUNC	15,535	150.9	307.3	No	GRAPH	10-TASK CLASSIF.	AVG. PRECISION
PCQM-CONTACT	529,434	30.1	61.0	No	INDUCTIVE LINK	LINK RANKING	MRR
PEPTIDES-STRUCT	15,535	150.9	307.3	No	GRAPH	11-TASK REGRESSION	MEAN ABS. ERROR
OGBG-MOLPCBA	437,929	26.0	28.1	No	GRAPH	128-TASK CLASSIF.	AVG. PRECISION
OGBG-PPA	158,100	243.4	2,266.1	No	GRAPH	37-TASK CLASSIF.	ACCURACY
OGBG-CODE2	452,741	125.2	124.2	YES	GRAPH	5 TOKEN SEQUENCE	F1 SCORE

Table 7: Summary of the datasets for transductive node classification [38, 28] used in this study.

DATASET	HOMOPHILY SCORE	# NODES	# EDGES	# CLASSES	METRIC
ROMAN-EMPIRE	0.023	22,662	32,927	18	ACCURACY
AMAZON-RATINGS	0.127	24,492	93,050	5	ACCURACY
MINESWEEPER	0.009	10,000	39,402	2	ROC AUC
TOLOKERS	0.187	11,758	519,000	2	ROC AUC
QUESTIONS	0.072	48,921	153,540	2	ROC AUC
POKEC	0.000	1,632,803	30,622,564	2	ACCURACY

PATTERN and CLUSTER (MIT License) [13]. PATTERN and CLUSTER are synthetic graph datasets constructed using the Stochastic Block Model (SBM). They offer a unique challenge for inductive node-level classification, where the goal is to predict the class label of unseen nodes. PATTERN: This dataset presents the task of identifying pre-defined sub-graph patterns (100 possible) embedded within the larger graph. These embedded patterns are generated from distinct SBM parameters compared to the background graph, requiring the model to learn these differentiating connection characteristics. CLUSTER: Each graph in CLUSTER consists of six pre-defined clusters generated using the same SBM distribution. However, only one node per cluster is explicitly labeled with its unique cluster ID. The task is to infer the cluster membership (ID) for all remaining nodes based solely on the graph structure and node connectivity information.

PASCALVOC-SP and COCO-SP (Custom license for Pascal VOC 2011 respecting Flickr terms of use, and CC BY 4.0 license) [15]. PascalVOC-SP and COCO-SP are graph datasets derived from the popular image datasets Pascal VOC and MS COCO, respectively. These datasets leverage SLIC superpixelization, a technique that segments images into regions with similar properties. In both datasets, each superpixel is represented as a node in a graph, and the classification task is to predict the object class that each node belongs to.

PEPTIDES-FUNC and PEPTIDES-STRUCT (CC BY-NC 4.0) [15]. Peptides-func and Peptides-struct offer complementary views of peptide properties by leveraging atomic graphs derived from the SATPdb database. Peptides-func focuses on multi-label graph classification, aiming to predict one or more functional classes (out of 10 non-exclusive categories) for each peptide. In contrast, Peptides-struct employs graph regression to predict 11 continuous 3D structural properties of the peptides.

PCQM-CONTACT (CC BY 4.0) [15]. The PCQM-Contact dataset builds upon PCQM4Mv2 [22] by incorporating 3D molecular structures. This enables the task of binary link prediction, where the goal is to identify pairs of atoms (nodes) that are considered to be in close physical proximity (less than 3.5 angstroms) in 3D space, yet appear far apart (more than 5 hops) when looking solely at the 2D molecular graph structure. The standard evaluation metric for this ranking task is Mean Reciprocal Rank (MRR). As noticed by [44], the original implementation by [15] suffers from false negatives and self-loops. Thus, we use the filtered version of the MRR provided by [44].

OGBG-MOLPCBA (MIT License) [22]. The ogbg-molpcba dataset, incorporated by the Open Graph Benchmark (OGB) [22] from MoleculeNet, focuses on multi-task binary classification of

molecular properties. This dataset leverages a standardized node (atom) and edge (bond) feature representation that captures relevant chemophysical information. Derived from PubChem BioAssay, ogbg-molpcba offers the task of predicting the outcome of 128 distinct bioassays, making it valuable for studying the relationship between molecular structure and biological activity.

OGBG-PPA (CC-0 license) [22]. The PPA dataset, introduced by OGB [22], focuses on species classification. This dataset represents protein-protein interactions within a network, where each node corresponds to a protein and edges denote associations between them. Edge attributes provide additional information about these interactions, such as co-expression levels. We employ the standard dataset splits established by OGB [22] for our analysis.

OGBG-CODE2 (MIT License) [22]. CODE2 [22] is a dataset containing source code from the Python programming language. It is made up of Abstract Syntax Trees where the task is to classify the sub-tokens that comprise the method name. We use the standard splits provided by OGB [22].

ROMAN-EMPIRE (MIT License) [38]. This dataset creates a graph from the Roman Empire Wikipedia article. Each word becomes a node, and edges connect words that are either sequential in the text or grammatically dependent (based on the dependency tree). Nodes are labeled by their syntactic role (17 most frequent roles are selected as unique classes and all the other roles are grouped into the 18th class). We use the standard splits provided by [38].

AMAZON-RATINGS (MIT License) [38]. Based on the Amazon product co-purchase data, this dataset predicts a product’s average rating (5 classes). Products (books, etc.) are nodes, connected if frequently bought together. Mean fastText embeddings are used for product descriptions as node features and focus on the largest connected component for efficiency (5-core). We use the standard splits provided by [38].

MINESWEEPER (MIT License) [38]. This is a synthetic dataset with a regular 100x100 grid where nodes represent cells. Each node connects to its eight neighbors (except edges). 20% of nodes are randomly mined. The task is to predict which are mines. Node features are one-hot-encoded numbers of neighboring mines, but are missing for 50% of nodes (marked by a separate binary feature). This grid structure differs from other datasets due to its regularity (average degree: 7.88). Since mines are random, both adjusted homophily and label informativeness are very low. We use the standard splits provided by [38].

TOLOKERS (MIT License) [38]. This dataset features workers (nodes) from crowdsourcing projects. Edges connect workers who have collaborated on at least one of the 13 projects. The task is to predict banned workers. Node features include profile information and performance statistics. This graph (11.8K nodes, avg. degree 88.28) is significantly denser compared to other datasets. We use the standard splits provided by [38].

QUESTIONS (MIT License) [38]. This dataset focuses on user activity prediction. Users are nodes, connected if they answered each other’s questions (Sept 2021 - Aug 2022). The task is to predict which users remained active. User descriptions (if available) are encoded using fastText embeddings. Notably, 15% lack descriptions and are identified by a separate feature. We use the standard splits provided by [38].

POKEC (unknown License) [28]. This dataset was retrieved from SNAP [28] and preprocessed by [29]. The dataset contains anonymized data of the whole network of Pokec, the most popular online social network in Slovakia which has been provided for more than 10 years and connects more than 1.6 million people. Profile data contains gender, age, hobbies, interests, education, etc, and the task is to predict the gender. The dataset was not released with a license. Thus, we only provide numerical values without any raw texts from the dataset.

D.2 Computing details

We implemented our models using PyTorch Geometric [17] (MIT License). Experiments were conducted on a shared computing cluster with various CPU and GPU configurations, including a mix

Table 8: Hyperparameters for the 5 datasets from GNN Benchmarks [13].

HYPERPARAMETER	ZINC	MNIST	CIFAR10	PATTERN	CLUSTER
# BLOCKS	3	3	3	3	16
HIDDEN DIM	80	80	80	80	32
SEQUENCE LAYER	MAMBA (BIDIRECTIONAL)				
LOCAL MESSAGE PASSING	GIN				
GLOBAL MESSAGE PASSING	VN	NONE	NONE	VN	VN
DROPOUT	0.0	0.0	0.0	0.0	0.0
GRAPH POOLING	SUM	MEAN	MEAN	-	-
RW SAMPLING RATE	1.0	0.5	0.5	0.5	0.5
RW LENGTH	50	50	50	100	200
RW POSITION ENCODING WINDOW SIZE	8	8	8	16	32
BATCH SIZE	50	32	32	32	32
LEARNING RATE	0.002	0.002	0.002	0.002	0.01
# EPOCHS	500	100	100	100	100
# WARMUP EPOCHS	50	5	5	5	5
WEIGHT DECAY	0.0	1E-6	1E-6	0.0	0.0
# PARAMETERS	502K	474K	474K	504K	525K
TRAINING TIME (EPOCH/TOTAL)	16s/2.1H	130s/3.6H	160s/4.4H	57s/1.6H	241s/6.7H

Table 9: Hyperparameters for the 5 datasets from LRGB [15].

HYPERPARAMETER	PASCALVOC-SP	COCO-SP	PEPTIDES-FUNC	PEPTIDES-STRUCT	PCQM-CONTACT
# BLOCKS	5	6	6	6	3
HIDDEN DIM	56	56	56	56	80
SEQUENCE LAYER	MAMBA (BIDIRECTIONAL)				
LOCAL MESSAGE PASSING	GIN				
GLOBAL MESSAGE PASSING	TRANS.	NONE	VN	VN	VN
DROPOUT	0.0	0.0	0.0	0.0	0.0
GRAPH POOLING	-	-	MEAN	MEAN	-
RW SAMPLING RATE	0.5	0.25	0.5	0.5	0.5
RW LENGTH	100	100	100	100	75
RW POSITION ENCODING WINDOW SIZE	16	16	16	32	16
BATCH SIZE	32	32	32	32	256
LEARNING RATE	0.002	0.002	0.002	0.004	0.001
# EPOCHS	200	200	200	200	150
# WARMUP EPOCHS	10	10	10	10	10
WEIGHT DECAY	1E-06	0.0	0.0	0.0	0.0
# PARAMETERS	531K	492K	530K	541K	505K
TRAINING TIME (EPOCH/TOTAL)	218s/12H	1402s/78H	112s/6.2H	112s/6.2H	528s/22H

of NVIDIA A100 (40GB) and H100 (80GB) GPUs. Each experiment was allocated resources on a single GPU, along with 4-8 CPUs and up to 60GB of system RAM. The run-time of each model was measured on a single NVIDIA A100 GPU.

D.3 Hyperparameters

Given the large number of hyperparameters and datasets, we did not perform an exhaustive search beyond the ablation studies in Section 5.2. For each dataset, we then adjusted the number of layers, the hidden dimension, the learning rate, the weight decay based on hyperparameters reported in the related literature [39, 45, 11, 44].

For the datasets from Benchmarking GNNs [13] and LRGB [15], we follow the commonly used parameter budgets of 500K parameters.

For the node classification datasets from [38] and [28], we strictly follow the experimental setup from the state-of-the-art method Polynormer [11]. We only replace the global attention blocks from Polynormer with NeuralWalker’s walk encoder blocks and use the same hyperparameters selected by Polynormer [11].

We use the AdamW optimizer throughout our experiments with the default beta parameters in Pytorch. We use a linear warm-up increase of the learning rate at the beginning of the training followed by its cosine decay as in [39]. The test sampling rate is always set to 1.0 if not specified. The detailed hyperparameters used in NeuralWalker as well as the model sizes and runtime on different datasets are provided in Table 8, 9, 10, and 11.

Table 10: Hyperparameters for the 3 datasets from OGB [22].

HYPERPARAMETER	OGBG-MOLPCBA	OGBG-PPA	OGBG-CODE2
# BLOCKS	4	1	3
HIDDEN DIM	500	384	256
SEQUENCE LAYER	CONV.	CONV.	CONV.
LOCAL MESSAGE PASSING	GATEDGCN	GIN	GIN
GLOBAL MESSAGE PASSING	VN	PERFORMER	TRANS.
DROPOUT	0.4	0.4	0.0
GRAPH POOLING	MEAN	MEAN	MEAN
RW SAMPLING RATE	0.5	0.5	0.5
RW LENGTH	25	200	100
RW POSITION ENCODING WINDOW SIZE	8	32	64
BATCH SIZE	512	32	32
LEARNING RATE	0.002	0.002	0.0003
# EPOCHS	100	200	30
# WARMUP EPOCHS	5	10	2
WEIGHT DECAY	0.0	0.0	0.0
# PARAMETERS	13.0M	3.1M	12.5M
TRAINING TIME (EPOCH/TOTAL)	226s/6.3H	671s/37H	1597s/13.3H

Table 11: Hyperparameters for node classification datasets from [38] and [28]. The other hyperparameters strictly follow Polynormer [11].

HYPERPARAMETER	ROMAN-EMPIRE	AMAZON-RATINGS	MINESWEEPER	TOLOKERS	QUESTIONS	POKEC
SEQUENCE LAYER			MAMBA			CONV.
DROPOUT	0.3	0.2	0.3	0.1	0.2	0.1
RW SAMPLING RATE	0.01	0.01	0.01	0.01	0.01	0.001
RW TEST SAMPLING RATE	0.1	0.1	0.1	0.1	0.05	0.001
RW LENGTH	1000	1000	1000	1000	1000	500
RW POSITION ENCODING WINDOW SIZE	8	8	8	8	8	8
LEARNING RATE	0.0005	0.0005	0.0005	0.001	5E-5	0.0005
TRAINING TIME (EPOCH/TOTAL)	0.50s/0.35H	0.6s/0.45H	0.22s/0.12H	0.67s/0.19H	0.67s/0.32H	6.44s/4.5H

D.4 Detailed Results and Robustness to Sampling Variability

Since NeuralWalker’s output depends on the sampled random walks, we evaluate its robustness to sampling variability. Following Tonshoff et al. (2023) [45], we measure the local standard deviation (local std) by computing the standard deviation of performance metrics obtained with five independent sets of random walks (details in [45]). The complete results for all datasets are presented in Table 12. Notably, by comparing the local std to the cross-model std obtained from training different models with varying random seeds, we consistently observe a smaller local std. This finding suggests that NeuralWalker’s predictions are robust to the randomness inherent in the random walk sampling process.

Table 12: Detailed results for all the datasets. Note that different metrics are used to measure the performance on the datasets. For each experiment, we provide the cross-model std using different random seeds and the local std using different sets of random walks.

DATASET	METRIC	TEST			VALIDATION	
		SCORE	CROSS MODEL STD	LOCAL STD	SCORE	CROSS-MODEL STD
ZINC	MAE	0.0646	0.0007	0.0005	0.0782	0.0038
MNIST	ACC	0.9876	0.0008	0.0003	0.9902	0.0006
CIFAR10	ACC	0.8003	0.0019	0.0009	0.8125	0.0053
PATTERN	ACC	0.8698	0.0001	0.0001	0.8689	0.0003
CLUSTER	ACC	0.7819	0.0019	0.0004	0.7827	0.0007
PASCALVOC-SP	F1	0.4912	0.0042	0.0019	0.5053	0.0084
COCO-SP	F1	0.4398	0.0033	0.0011	0.4446	0.0030
PEPTIDES-FUNC	AP	0.7096	0.0078	0.0014	0.7145	0.0033
PEPTIDES-STRUCT	AP	0.2463	0.0005	0.0004	0.2389	0.0021
PCQM-CONTACT	MRR	0.4707	0.0007	0.0002	0.4743	0.0006
OGBG-MOLPCBA	AP	0.3086	0.0031	0.0010	0.3160	0.0032
OGBG-PPA	ACC	0.7888	0.0059	0.0004	0.7460	0.0058
OGBG-CODE2	F1	0.1957	0.0025	0.0005	0.1796	0.0031
ROMAN-EMPIRE	ACC	0.9292	0.0036	0.0005	0.9310	0.0032
AMAZON-RATINGS	ACC	0.5458	0.0036	0.0009	0.5491	0.0049
MINESWEEPER	ROC AUC	0.9782	0.0040	0.0003	0.9794	0.0047
TOLOKERS	ROC AUC	0.8556	0.0075	0.0010	0.8540	0.0096
QUESTIONS	ROC AUC	0.7852	0.0113	0.0009	0.7902	0.0086
POKEC	ACC	0.8646	0.0009	0.0001	0.8644	0.0003